Two-Dimensional birefringence imaging in biological tissue using polarization sensitive optical coherence tomography.

Johannes F. de Boer[a], Thomas E. Milner[a], Martin J. C. van Gemert[b] and J. Stuart Nelson[a]

[a]Beckman Laser Institute and Medical Clinic, University of California, Irvine, 1002 Health Sciences Road East, Irvine, California 92612, USA

[b]Laser Center, Academic Medical Center, Meibergdreef 9, 1105 AZ Amsterdam, The Netherlands

ABSTRACT

Using a polarization sensitive Michelson interferometer, we measure two-dimensional images of optical birefringence in bovine tendon as a function of depth with a technique known as Optical Coherence Tomography (OCT). Detection of the polarization state of the signal, formed by interference of backscattered light from the sample and a mirror in the reference arm, gives the optical phase delay between light that has propagated along the fast and slow axes of the birefringent tendon. Images showing the change in birefringence in response to laser irradiation are presented. The technique allows rapid non-contact investigation of tissue structural properties through two-dimensional imaging of birefringence.

Keywords: Optical Coherence Tomography, Birefringence, Imaging

1. INTRODUCTION

The demand for non-invasive optical imaging in biological tissue has led to the development of several techniques to circumvent the common problem of scattering in turbid media; such techniques include diffusing wave spectroscopy,[1] time-gated imaging using snake-like photons,[2] two-photon fluorescence imaging,[3] ultrasonic modulation of diffusing waves[4,5] and optical coherence tomography[6,7] (OCT).

OCT uses the partial coherence properties of a light source to image structures with high resolution ($1-15\ \mu m$) in turbid media such as biological tissue. The sample is positioned in one arm (the sample arm) of a two-beam interferometer. Interference fringes are formed when the optical path length of light backscattered from the sample matches that from the reference arm to within the coherence length of the source light. The optical path length in the reference arm acts as a coherence gate on the detection, selecting only light backscattered from the sample that has traveled the same optical path length. By lateral and longitudinal scanning, two-dimensional (2D) OCT images are constructed that map the amplitude of light backscattered from the sample. Lateral resolution is determined by the spot size of the beam focus of incoming light and the collection aperture; longitudinal resolution is determined by the coherence length of source light.

We present a combination of OCT and polarization sensitive detection[8] to record 2D images of the change in polarization of circularly polarized incoming light backscattered from a turbid birefringent sample. In contrast to conventional OCT, in which the amplitude of backscattered light in a single polarization state is measured, we detected both polarization states to characterize the sample birefringence as a function of depth. 2D maps of birefringence of biological materials can reveal important structural information that is difficult to resolve with other imaging techniques. Partial loss of birefringence is known to be an early indication of tissue thermal damage[9] (e.g., burns, or laser treatments). To demonstrate polarization-sensitive OCT, we present 1 mm and 1.5 mm wide by 700 μm deep images of bovine tendon birefringence before and after pulsed laser irradiation. For comparison reflection OCT images are shown, formed by the sum of both detected polarization channels. Figure 1 shows a schematic of the polarization-sensitive OCT system used in our experiments. Light passes through a Glan-Thompson

Corresponding author: JFdB, Email: deboer@bli.uci.edu; Telephone: 714-824-3284; Fax: 714-824-8413

A color version of this and other articles can be downloaded at http://www.bli.uci.edu/research/jd/deboer.html

SPIE Vol. 3196 • 0277-786X/98/$10.00

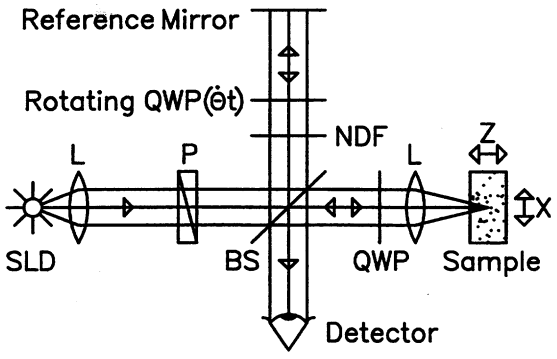

Figure 1. Schematic of the polarization sensitive OCT system. *SLD*: superluminescent diode, 0.8 mW output power, central wavelength $\lambda_0 = 862\ nm$ and spectral FWHM $\Delta\lambda = 21\ nm$ $(= \lambda_0^2\,\Omega\sqrt{\ln 2}/\pi c)$; *P*: polarizer; *BS*: beamsplitter; *QWP*: quarter wave plate; *NDF*: neutral density filter; *L*: lens. 2D images are formed by longitudinal movement of the sample with constant velocity $v = 1\ mm/s$ (z-direction), repeated after each 10 μm lateral displacement (x-direction).

polarizer to select a pure linear vertical input state and is split into the reference and sample arms by a polarization insensitive beamsplitter (reflection and transmission coefficients for linear vertical and horizontal polarization states were 0.5 ± 0.05). Light in the reference arm passes through a zero-order quarter wave plate (QWP), rotating at $\dot{\Theta} = 200\pi\ rad/s$. Following reflection from a planar mirror and a return pass through the QWP, the light has a rotating linear polarization ($400\pi\ rad/s$). For improved signal-noise ratio,[10] a neutral density filter NDF positioned in the reference arm reduces intensity noise 50 times. Light in the sample arm passes through a QWP oriented at 45^0 to the incident vertical polarization to give circularly polarized light incident on the tendon. After double passage through a lens, sample, and the QWP, the light is in an arbitrary (elliptical) polarization state, determined by the sample birefringence.

2. THEORY

The intensity of the light incident upon the detector is given by recombination of the light in both arms of the interferometer,

$$\langle I\rangle = \langle I_r\rangle + \langle I_s\rangle + 2\mathrm{Re}\left[\langle\vec{\Psi}_r^*(t,z_r)\cdot\vec{\Psi}_s(t,z_s)\rangle\right] \tag{1}$$

where $\vec{\Psi}(t,z)$ is the light amplitude field vector, subscripts r and s denote the reference and sample arms, respectively, $z_{r,s}$ are the optical path lengths in reference or sample arms, and the angle brackets denote ensemble averaging. The source spectral density $S(\omega)$ is assumed to be Gaussian ($\propto \exp[-(\omega-\omega_0)^2/\Omega^2]$) with FWHM $= 2\Omega\sqrt{\ln 2}\ rad/s$. The evolution of the polarization state in each arm of the interferometer is computed with the Jones matrix formalism, where we neglect optical dispersion in the sample and spectral dependence of the zero order QWP's over the spectrum of the source. The interference fringe intensity formed by light in the sample and reference arms can be separated into horizontal A_H and vertical A_V polarization components that are proportional to the light amplitude fields backscattered from the sample:

$$\begin{aligned}
&\mathrm{Re}\left[\langle\vec{\Psi}_r^*(t,z_r)\cdot\vec{\Psi}_s(t,z_s)\rangle\right] = A_H + A_V;\\
&A_H \approx \sin(2\dot{\Theta}t)\cos(2k_0\Delta z)\ \exp[-(\Omega\Delta z/c)^2]\cos(k_0 z\delta),\\
&A_V \approx \cos(2\dot{\Theta}t)\cos(2k_0\Delta z{+}2\alpha)\ \exp[-(\Omega\Delta z/c)^2]\sin(k_0 z\delta),
\end{aligned} \tag{2}$$

where Δz is the optical path-length difference between the sample and the reference arms of the interferometer. In our system Δz is a function of time and longitudinal velocity of the sample; z is the backscatter depth in the sample; $k_0 = 2\pi/\lambda_0$; c is the speed of light in vacuum; δ is the difference in refractive indices along the fast and slow axes of the birefringent sample $(n_s - n_f)$; $\dot{\Theta}$ is the rotation speed of the QWP in the reference arm and α is the angle of the fast optical axis of the birefringent sample with the horizontal. The only approximation in Eq. (2) is that

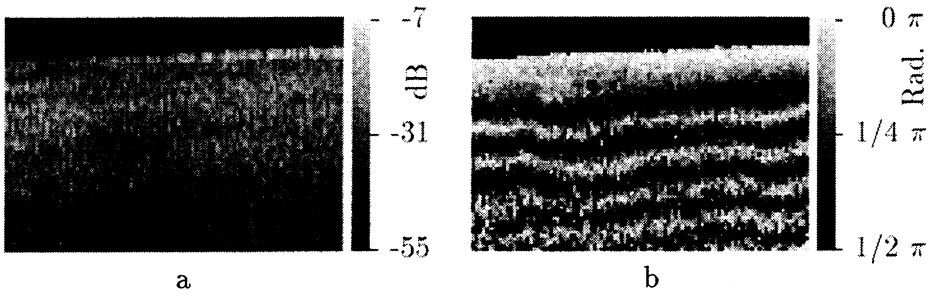

Figure 2. Images of fresh bovine tendon 1 *mm* wide by 700 μm deep, constructed from the same measurement. a) Conventional reflection image generated by computing $10\log[I_H(z) + I_V(z)]$. The grey scale to the right gives the magnitude of the signals. b) Birefringence image, generated by computing the angle of rotation ϕ in Eq. (4). The grey scale at the right gives the angle ϕ. The banded structure, indicative of the birefringence, is clearly visible. Each pixel represents a 10 $\mu m \times 10$ μm area. The dynamic range of the system was 48 dB.

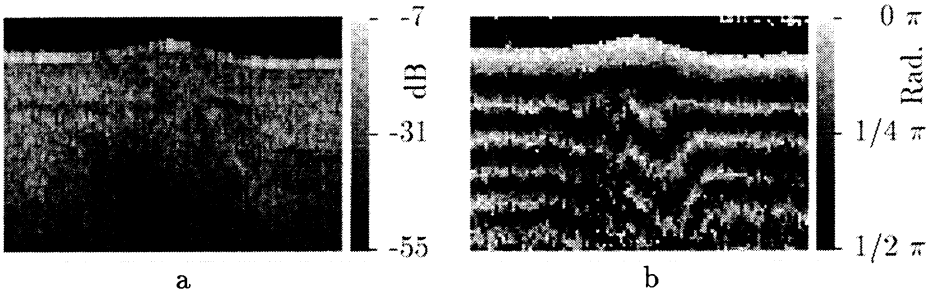

Figure 3. Images of fresh bovine tendon 1 *mm* wide by 700 μm deep, constructed from the same measurement. a) Conventional reflection image generated by computing $10\log[I_H(z) + I_V(z)]$. The grey scale to the right gives the magnitude of the signals. b) Birefringence image generated by computing the angle of rotation ϕ in Eq. (4). The grey scale at the right gives the angle ϕ. The bovine tendon was exposed to three consecutive 1 Joule 150 μs laser pulses ($\lambda = 1.32$ μm) spaced by 10 *ms*, incident from the upper left at 35^0 with respect to the surface normal. The beam diameter was 2 *mm*. Initial surface temperature after laser irradiation was 77 ^0C, dropping to 61 ^0C after 0.25 sec. The displacement of the banded structure in the image indicates the loss of birefringence due to thermal damage in the irradiated zone. Each pixel represents a 10 $\mu m \times 10$ μm area.

the product of birefringence (δ) and propagation depth (z) in the sample (in the present case $z\delta \leq 2.6$ μm) is much smaller than the width of the coherence envelope ($2c/\Omega = 19$ μm). Phase sensitive demodulation of the recorded signal with respect to angular position of the rotating QWP ($\dot{\Theta}t$) permits separation of the intensities corresponding to vertically and horizontally polarized light. In addition to the carrier frequency $[\cos(2k_0\Delta z)]$ within the coherence envelope $\{\exp[-(\Omega\Delta z/c)^2]\}$ both signals show an oscillation with a periodicity determined by the product of sample birefringence (δ) and propagation depth (z) that allows for birefringence imaging.

3. EXPERIMENT

We made scans by moving the sample at constant velocity $v = 1$ mm/s, giving a carrier frequency $\nu = 2v/\lambda_0 = 2.4$ kHz. To form 2D images, we recorded a longitudinal scan after each 10 μm lateral displacement of the sample. The 4 *mm* diameter beam, focused upon a sample by a lens ($f = 50.2$ *mm*) gave a 14 μm beam-waist diameter. In air, the sample arm was matched in length to the reference arm at a position 200 μm past the focal point, leading to a matched length in the beam focus approximately 400 μm deep in a sample with refractive index $n = 1.4$ (Ref. 11,12). The detector was AC coupled and the signal amplified, high-pass filtered at 1 kHz with 18-dB/octave roll-off and digitized with 16 bit resolution at 50,000 points per second. Signal processing consisted of squaring the detected signal and phase sensitive demodulation with respect to $\dot{\Theta}t$ to separate the horizontal I_H and vertical I_V components of the backscattered light. Then, within each longitudinal scan, data points were averaged with a Gaussian weight function (FWHM = 700 data points) to form one image pixel. The resulting signals gave the backscattered horizontal

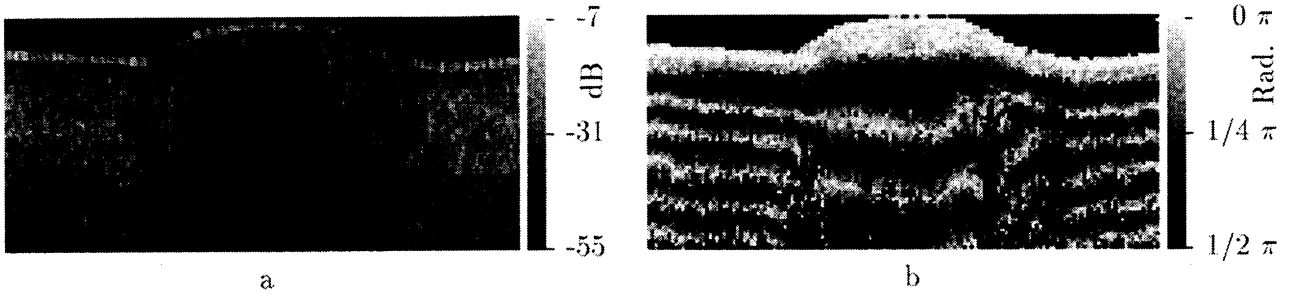

Figure 4. Images of fresh bovine tendon 1.5 *mm* wide by 700 μm deep, constructed from the same measurement. a) Conventional reflection image generated by computing $10\log[I_H(z) + I_V(z)]$. The grey scale to the right gives the magnitude of the signals. b) Birefringence image generated by computing the angle of rotation ϕ in Eq. (4). The grey scale at the right gives the angle ϕ. The bovine tendon was exposed to three consecutive 1.4 Joule 150 μs laser pulses ($\lambda = 1.32\ \mu m$) spaced by 10 *ms*, incident from the upper left at 35^0 with respect to the surface normal. The beam diameter was 2 *mm*. Initial surface temperature after laser irradiation was 88 ^0C, dropping to 70 ^0C after 0.25 sec. The displacement of the banded structure in the image indicates the loss of birefringence due to thermal damage in the irradiated zone. Each pixel represents a 10 $\mu m \times 10\ \mu m$ area.

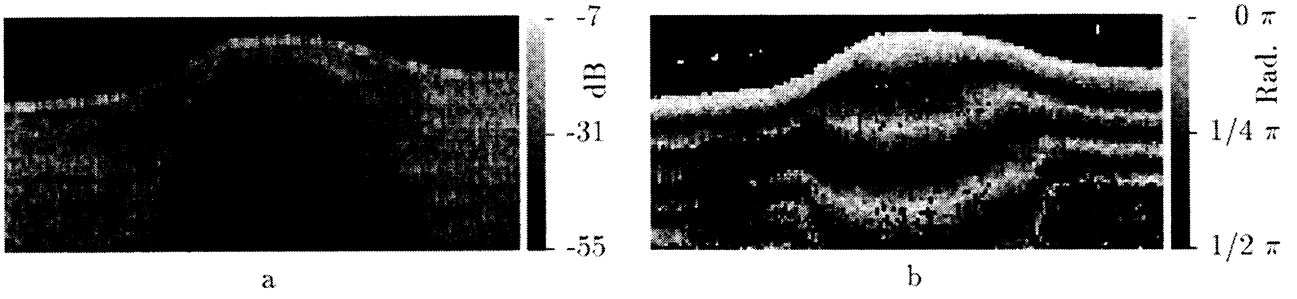

Figure 5. Images of fresh bovine tendon 1.5 *mm* wide by 700 μm deep, constructed from the same measurement. a) Conventional reflection image generated by computing $10\log[I_H(z) + I_V(z)]$. The grey scale to the right gives the magnitude of the signals. b) Birefringence image generated by computing the angle of rotation ϕ in Eq. (4). The grey scale at the right gives the angle ϕ. The bovine tendon was exposed to three consecutive 1.5 Joule 150 μs laser pulses ($\lambda = 1.32\ \mu m$) spaced by 10 *ms*, incident from the upper left at 35^0 with respect to the surface normal. The beam diameter was 2 *mm*. Prior to exposure to the laser irradiation the surface was cooled to -5 ^0C in 40 msec. Maximum surface temperature of 68 ^0C was reached 330 msec. after laser irradiation. The displacement of the banded structure in the image indicates the loss of birefringence due to thermal damage in the irradiated zone. Compared to Fig. 4 the loss of birefringence at the surface is smaller, attributed to the lower thermal damage due to surface cooling. Each pixel represents a 10 $\mu m \times 10\ \mu m$ area.

and vertical intensities as a function of depth z with a resolution of 10 μm physical distance, modulated with their respective birefringence dependent terms:

$$I_H(z) \propto \cos^2(k_0 z\delta); \qquad I_V(z) \propto \sin^2(k_0 z\delta). \tag{3}$$

The birefringence images were formed by calculating the angle ϕ of the polarization rotation,

$$\phi = \arctan\sqrt{\frac{I_V(z)}{I_H(z)}} = k_0 z\delta, \tag{4}$$

and the conventional reflection OCT images were formed by the sum of both polarization channels,

$$I_b(z) = I_H(z) + I_V(z). \tag{5}$$

4. RESULTS

Measurements on 1 $cm \times 2$ cm samples at least 1 cm thick were done within 48 hours of bovine sacrifice. In Fig. 2 conventional and birefringence images of fresh bovine tendon are shown. The banded structure in Fig. 2b, indicative of birefringence, is clearly visible up to a physical depth of $700\mu m$, while this structure is completely absent in the conventional reflection image in Fig. 2a. This shows that the banded structure in the birefringence image is not an anatomical artefact in the tendon, but due solely to its birefringence. By measuring the optical-versus-physical thickness of a thin slice,[11] we found the average refractive index of the tendon to be $\bar{n} = 1.42 \pm 0.03$. We determined the birefringence by the average distance between the first and second dark bands from the top of Fig. 2b over the full width (100 lateral scans). The average distance $\bar{z} = 116 \pm 13$ μm corresponded to a polarization rotation $\phi = k_0 \bar{z} \delta = \pi$ in Eq. (4). The experimentally determined birefringence $\delta = 3.7 \pm 0.4 \times 10^{-3}$ of bovine tendon (predominantly type I collagen) is in agreement with reported values of $3.0 \pm 0.6 \times 10^{-3}$ (Ref. 13) and $2.8-3.0 \times 10^{-3}$(Ref. 14,15). Fitting $\exp(-2z/\gamma)$, between $z = 150 - 600$ μm depth, to the total backscattered intensity in the sample, $I_b(z)$ in Eq. (5), averaged over the image in Fig 2a (100 lateral scans), gave $\gamma \approx 0.2$ mm. Decay of total backscattered light intensity with depth depends on several factors, among them attenuation of the coherent beam by scattering and the geometry of the collection optics.

In Fig. 3 conventional and birefringence images of laser irradiated bovine tendon are presented. The image clearly shows a decrease in the birefringence at the center of the irradiation zone, extending into the tendon over the full depth of the image (700 μm). Furthermore, the direction of incoming laser light (from the upper left corner, at an angle of 35^0 with the normal of the surface) is observed. The surface temperature of the tendon was monitored during laser irradiation by IR radiometry. For comparison, Fig. 3a shows an OCT image of the total backscattered intensity $I_b(z)$. Although less backscattered light from the irradiated area can be observed, the polarization sensitive image (Fig. 3b) reveals important structural information not evident in Fig. 3a. In Figs. 4 and 5 conventional and birefringence images 1.5 mm wide by 700 μm deep are presented of laser irradiated tendon with and without surface cooling. Since loss of birefringence is attributed to thermal damage, comparison of the two figures shows the effect of surface cooling on laser mediated thermal damage. Application of cooling clearly reduces the birefringence loss near the surface in Fig. 5 as compared to Fig. 4.

5. CONCLUSIONS

We have shown that polarization-sensitive OCT can reveal structural information in birefringent turbid media such as biological tissue that is not available when polarization-insensitive OCT is used. Polarization-sensitive OCT has the potential to provide guidance regarding optimal dosimetry for thermally mediated laser therapeutic procedures by permitting real-time diagnostics at each irradiated site through detection of changes in birefringence associated with thermal damage and pathological conditions. This would permit a semiquantitative evaluation of the efficacy of laser therapy as a function of incident light dosage. Since many biological tissues are birefringent (e.g. collagen, the constituent of bovine tendon, is also present in skin, bone, cornea, cartilage and the cardiovascular system), polarization sensitive OCT is important even for conventional reflectance OCT. Reflection images can show pseudo structure when tissue birefringence rotates backscattered light to the polarization state perpendicular to the detected channel. Only detection of both polarization channels gives a true reflectance OCT image in birefringent biological tissue.

Research grants from The Biomedical Research Technology Program and the Institute of Arthritis and Musculoskeletal and Skin Diseases of The National Institutes of Health, the Whitaker Foundation (WF 21025) and the Dermatology Foundation are gratefully acknowledged, as is Institute support from the U.S. Department of Energy, the National Institutes of Health, and the Beckman Laser Institute Endowment. In addition, J. F. de Boer and M. J. C.van Gemert gratefully acknowledge financial support from the Dutch Technology Foundation (STW, grants AGN 33.2954 and AGN 55.3906) and the Academic Medical Center. This article is an extended version of Ref. 16.

REFERENCES

1. A. Yodh and B. Chance, "Spectroscopy and imaging with diffuse light," *Physics Today* **48**, pp. 34–40, Mar. 1995.
2. F. Liu, K. M. Yoo, and R. R. Alfano, "Transmitted photon intensity through biological tissues within various time windows," *Optics Letters* **19**, pp. 740–742, May 1994.
3. W. Denk, D. W. Piston, and W. W. Webb in *Handbook of Biological Confocal Microscopy*, J. B. Pawley, ed., p. 445, Plenum, New York, 1995.
4. L. Wang, S. L. Jacques, and X. Zhao, "Continuous-wave ultrasonic modulation of scattered laser light to image objects in turbid media," *Optics Letters* **20**, pp. 629–631, Mar. 1995.
5. M. Kempe, M. Larionov, D. Zaslavsky, and A. Z. Genack, "Acousto-optic tomography with multiple scattered light," *J. Opt. Soc. Am. A* **14**, pp. 1151–1158, May 1997.
6. D. Huang, E. A. Swanson, C. P. Lin, J. S. Schuman, W. G. Stinson, W. Chang, M. R. Hee, T. Flotte, K. Gregory, C. A. Puliafito, and J. G. Fujimoto, "Optical coherence tomography," *Science* **254**, pp. 1178–1181, Nov. 1991.
7. A. F. Fercher, "Optical coherence tomography," *J. Biomed. Opt.* **1**, pp. 157–173, Apr. 1996.
8. M. R. Hee, D. Huang, E. A. Swanson, and J. G. Fujimoto, "Polarization-sensitive low-coherence reflectometer for birefringence characterization and ranging," *J. Opt. Soc. Am. B* **9**, pp. 903–908, June 1992.
9. S. Thomsen, "Pathologic analysis of photothermal and photomechanical effects of laser-tissue interactions," *Photochem. Photobiol* **53**(6), pp. 825–835, 1991.
10. W. V. Sorin and D. M. Baney, "A simple intensity noise reduction technique for optical low-coherence reflectometry," *IEEE Photonics Tech. Lett.* **4**, pp. 1404–1406, Dec. 1992.
11. G. J. Tearney, M. E. Brezinski, J. F. Southern, B. E. Bouma, M. R. Hee, and J. G. Fujimoto, "Determination of the refractive index of highly scattering human tissue by optical coherence tomography," *Optics Letters* **20**, pp. 2258–2260, Nov. 1995.
12. Z. Chen, T. E. Milner, D. Dave, and J. S. Nelson, "Optical doppler tomographic imaging of fluid flow velocity in highly scattering media," *Optics Letters* **22**, pp. 64–66, Jan. 1997.
13. D. J. Maitland and J. T. Walsh, "Quantitative measurements of linear birefringence during heating of native collagen," *Lasers Surg. Med.* **20**(3), pp. 310–318, 1997.
14. E. P. Chang, D. A. Keedy, and C. W. Chien, "Ultrastructures of rabbit corneal stroma: Mapping of optical and morphological anisotropies," *Biochim. Biophys. Acta* **343**, pp. 615–626, May 1974.
15. E. J. Naylor, "The structure of the cornea as revealed by polarized light," *Quart. J. Microsc. Sci.* **94**, pp. 83–88, Mar. 1953.
16. J. F. de Boer, T. E. Milner, M. J. C. van Gemert, and J. S. Nelson, "Two-dimensional birefringence imaging in biological tissue using polarization sensitive optical coherence tomography," *Optics Letters* **22**, pp. 934–936, June 1997.